Computers and Structures 164 (2016) 53–62

Contents lists available at ScienceDirect

Computers and Structures

journal homepage: www.elsevier.com/locate/compstruc

A simplified error estimator for the CB method and its application to error control

Seung-Hwan Boo [a], Jin-Gyun Kim [b], Phill-Seung Lee [a,*]

[a] Department of Mechanical Engineering, Korea Advanced Institute of Science and Technology, 291 Daehak-ro, Yuseong-gu, Daejeon 34141, Republic of Korea
[b] Mechanical Systems Safety Research Division, Korea Institute of Machinery and Materials, 156, Gajeongbuk-ro, Yuseong-gu, Daejeon 34103, Republic of Korea

ARTICLE INFO

Article history:
Received 17 July 2015
Accepted 4 November 2015

Keywords:
Structural dynamics
Finite element method
Model reduction
Component mode synthesis
Craig–Bampton method
Error estimation

ABSTRACT

In this paper, we simplify the error estimation technique developed for the Craig–Bampton (CB) method (Kim et al., 2014). The original formulation is simplified by neglecting insignificant terms, a new error estimator is obtained, and thus computational cost is significantly reduced with negligible accuracy loss. In addition, the contribution of a specific substructure to a relative eigenvalue error can be estimated using the new formulation, in which the estimated relative eigenvalue error is represented by a simple summation of the substructural errors estimated. Therefore, the new formulation can be employed for error control by using the detailed errors estimated for a certain substructure. Through various numerical examples, we verify the accuracy and computational efficiency of the new formulation, and demonstrate an error control strategy.

1. Introduction

In 1960s, component mode synthesis (CMS) was first presented by Hurty [2]. In the decades since then, various CMS methods have been developed [3–15]. The CMS methods have generally been employed to solve large and complex structural vibration problems efficiently, and their applications have been extended to new areas of research such as multi-body dynamics, structural health monitoring, structural design optimization, and real-time control of dynamic systems [16–19].

In CMS methods, one research issue is how to evaluate the reliability of eigensolutions obtained from the reduced model, when the exact eigensolutions are unknown. To handle this problem, several *a priori* and *a posteriori* error estimation methods have been developed [20–23]. Of special interest here, Elssel and Voss [21] developed an upper bound of the relative eigenvalue error for the automated multi-level substructuring (AMLS) method [24–26]. Since it is an *a priori* method and a scalar operation technique, it requires almost no computational cost. However, although it gives the tendency of the relative eigenvalue error as an upper bound, its estimation capability is not adequate for practical use in engineering problems.

Recently, an accurate error estimator was developed for the CB method using an enhanced transformation matrix derived considering the residual mode effect [1]. Its estimation accuracy and computational efficiency were tested with various structural finite element (FE) models (within 5000 DOFs). However, since the original formulation requires full matrix operations, its computational cost may become severe in problems with very large DOFs.

In order to improve its computational efficiency, we here propose a newly formulated error estimator extending the previous work [1]. First, the original formulation is simplified at the component matrix level and some higher order terms are neglected. Then, we newly define a simplified error estimator, in which the contribution of a specific substructure to a relative eigenvalue error can be calculated and the summation of the substructural eigenvalue errors is equal to the total eigenvalue error estimated. Consequently, using the simplified error estimator, we provide two important advantages (reduction of computational cost and capability to estimate substructural errors) with negligible loss of accuracy.

In particular, using the second feature, we can identify the substructural distribution of relative eigenvalue errors, which makes it possible to handle locally fluctuated eigenvalue errors by adjusting the number of substructural modes selected. It is important to note that the concept of the substructural error mentioned here nicely matches with the key idea of the component mode synthesis (CMS). That is, a whole model is the summation of its substructural models.

In the following sections, the CB method, the enhanced transformation matrix, and the previous error estimation method are

* Corresponding author.
E-mail address: phillseung@kaist.edu (P.S. Lee).

http://dx.doi.org/10.1016/j.compstruc.2015.11.003
0045-7949/

briefly reviewed. We then derive the simplified error estimator, and propose an error control strategy. Finally, the performance of the error estimator is tested using a variety of numerical examples.

2. Craig–Bampton method

In this section, we briefly introduce the formulation of the CB method, see Refs. [1–5] for detailed derivations.

Let us consider a global finite element model partitioned into n substructures fixed to its boundary interface, see Fig. 1. In the CB method, the equations of motion for free vibration are given

$$\mathbf{M}_g\ddot{\mathbf{u}}_g + \mathbf{K}_g\mathbf{u}_g = \mathbf{0}, \tag{1}$$

$$\mathbf{M}_g = \begin{bmatrix} \mathbf{M}_s & \mathbf{M}_c \\ \mathbf{M}_c^T & \mathbf{M}_b \end{bmatrix}, \quad \mathbf{K}_g = \begin{bmatrix} \mathbf{K}_s & \mathbf{K}_c \\ \mathbf{K}_c^T & \mathbf{K}_b \end{bmatrix}, \quad \mathbf{u}_g = \begin{bmatrix} \mathbf{u}_s \\ \mathbf{u}_b \end{bmatrix}, \tag{2}$$

where $\mathbf{M}$ and $\mathbf{K}$ are mass and stiffness matrices, respectively, $\mathbf{u}$ is the displacement vector, and $\ddot{(\,)} = d^2()/dt^2$ with time variable t. The subscript g denotes the global structural quantities, and the subscripts s and b denote the substructural and interface boundary quantities, respectively. The subscript c denotes the coupled quantities between substructures and interface boundary. Note that $\mathbf{M}_s$ and $\mathbf{K}_s$ are the block-diagonal mass and stiffness matrices that consist of substructural mass and stiffness matrices, $\mathbf{M}_i$ and $\mathbf{K}_i$ (for $i = 1, 2, \ldots, n$).

The eigenvalue problem for the global structure is defined as

$$\mathbf{K}_g(\boldsymbol{\varphi}_g)_i = \lambda_i\mathbf{M}_g(\boldsymbol{\varphi}_g)_i \quad \text{for } i = 1, 2, \ldots, N_g, \tag{3}$$

in which λ_i and $(\boldsymbol{\varphi}_g)_i$ are the eigenvalue and eigenvector corresponding to the ith global mode, and N_g is the number of DOFs in the global FE model. Note that $(\boldsymbol{\varphi}_g)_i$ is the mass-normalized eigenvector, and λ_i and $(\boldsymbol{\varphi}_g)_i$ satisfy mass-orthonormality and stiffness-orthogonality conditions.

Using the eigenvectors obtained from Eq. (3), the global displacement vector $\mathbf{u}_g$ is expressed by

$$\mathbf{u}_g = \boldsymbol{\Phi}_g\mathbf{q}_g, \tag{4a}$$

$$\text{with } \boldsymbol{\Phi}_g = \left[(\boldsymbol{\varphi}_g)_1 \;\; (\boldsymbol{\varphi}_g)_2 \;\; \cdots \;\; (\boldsymbol{\varphi}_g)_i\right], \mathbf{q}_g = \begin{bmatrix} \mathbf{q}_1 \\ \mathbf{q}_2 \\ \vdots \\ \mathbf{q}_i \end{bmatrix} \text{ for } i = 1, 2, \ldots, N_g, \tag{4b}$$

where $\boldsymbol{\Phi}_g$ is the global eigenvector matrix that contains the eigenvectors $(\boldsymbol{\varphi}_g)_i$ and $\mathbf{q}_g$ is the generalized coordinate vector that contains the generalized coordinates $\mathbf{q}_i$ corresponding to $(\boldsymbol{\varphi}_g)_i$.

Then, the transformation matrix $\mathbf{T}_0$ is constructed by combination of the fixed-interface normal modes $\boldsymbol{\Phi}$ and interface-constraint modes $\boldsymbol{\Psi}$ as

$$\mathbf{T}_0 = [\boldsymbol{\Phi} \quad \boldsymbol{\Psi}], \tag{5}$$

with

$$\boldsymbol{\Phi} = \begin{bmatrix} \boldsymbol{\Phi}_s \\ \mathbf{0} \end{bmatrix}, \quad \boldsymbol{\Psi} = \begin{bmatrix} \boldsymbol{\Psi}_c \\ \mathbf{I}_b \end{bmatrix}, \quad \boldsymbol{\Phi}_s = \begin{bmatrix} \boldsymbol{\Phi}_s^d & \boldsymbol{\Phi}_s^r \end{bmatrix}, \quad \boldsymbol{\Psi}_c = -\mathbf{K}_s^{-1}\mathbf{K}_c, \tag{6}$$

where $\boldsymbol{\Phi}_s$ is the block-diagonal eigenvector matrix that consists of substructural eigenvectors, and it is decomposed into $\boldsymbol{\Phi}_s^d$ and $\boldsymbol{\Phi}_s^r$ that are the eigenvector matrices corresponding to the dominant and residual substructural modes, respectively. Here, $\boldsymbol{\Psi}_c$ is the constraint modes matrix and $\mathbf{I}_b$ is an identity matrix for the interface boundary. The superscripts d and r denote the dominant and residual terms, respectively.

Then, $\boldsymbol{\Phi}_s$ is obtained using the following substructural eigenvalue problems

$$\mathbf{K}^{(i)}\boldsymbol{\Phi}^{(i)} = \boldsymbol{\Lambda}^{(i)}\mathbf{M}^{(i)}\boldsymbol{\Phi}^{(i)}, \quad \boldsymbol{\Phi}^{(i)} = [\boldsymbol{\Phi}_d^{(i)} \;\; \boldsymbol{\Phi}_r^{(i)}] \quad \text{for } i = 1, 2, \ldots, n, \tag{7}$$

where $\boldsymbol{\Phi}^{(i)}$ and $\boldsymbol{\Lambda}^{(i)}$ are the substructural eigenvector and eigenvalue matrices corresponding to the ith substructure, respectively. The substructural eigenvector matrix $\boldsymbol{\Phi}^{(i)}$ is decomposed into the dominant term $\boldsymbol{\Phi}_d^{(i)}$ and residual term $\boldsymbol{\Phi}_r^{(i)}$.

The constraint mode matrix $\boldsymbol{\Psi}_c$ in Eq. (6) is defined by

$$\boldsymbol{\Psi}_c = \begin{bmatrix} \boldsymbol{\Psi}_c^{(1)} \\ \boldsymbol{\Psi}_c^{(2)} \\ \vdots \\ \boldsymbol{\Psi}_c^{(i)} \end{bmatrix} \text{ with } \boldsymbol{\Psi}_c^{(i)} = -\left(\mathbf{K}^{(i)}\right)^{-1}\mathbf{K}_c^{(i)} \text{ for } i = 1, 2, \ldots, n, \tag{8}$$

in which $\boldsymbol{\Psi}_c^{(i)}$ is the constraint mode matrix of the ith substructure, and $\mathbf{K}_c^{(i)}$ is the stiffness matrix of the ith substructure coupled with the interface boundary. Here, $\left(\mathbf{K}^{(i)}\right)^{-1}$ is computed using the Cholesky factorization of $\mathbf{K}^{(i)}$.

Using the transformation matrix $\mathbf{T}_0$ in Eq. (5), the global displacement vector $\mathbf{u}_g$ is expressed by

$$\mathbf{u}_g = \begin{bmatrix} \mathbf{u}_s \\ \mathbf{u}_b \end{bmatrix} = \mathbf{T}_0\mathbf{u} \text{ with } \mathbf{T}_0 = \begin{bmatrix} \boldsymbol{\Phi}_s^d & \boldsymbol{\Phi}_s^r & \boldsymbol{\Psi}_c \\ \mathbf{0} & \mathbf{0} & \mathbf{I}_b \end{bmatrix}, \quad \mathbf{u} = \begin{bmatrix} \mathbf{q}_s^d \\ \mathbf{q}_s^r \\ \mathbf{u}_b \end{bmatrix}, \tag{9}$$

in which $\mathbf{q}_s^d$ and $\mathbf{q}_s^r$ are the generalized coordinate vectors corresponding to the dominant and residual substructural modes, respectively.

Neglecting the residual terms in $\mathbf{T}_0$ in Eq. (9), the global displacement vector $\mathbf{u}_g$ is approximated by

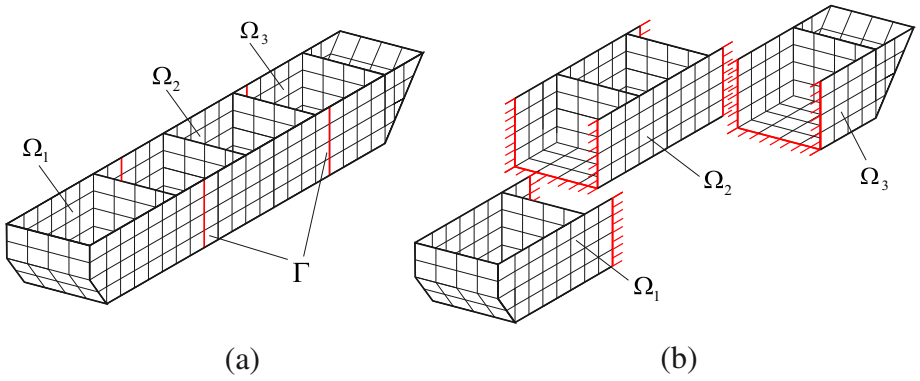

Fig. 1. Interface handling in the CB method: (a) partitioned structure and (b) fixed interface boundary treatment.

$$\mathbf{u}_g \approx \bar{\mathbf{u}}_g = \bar{\mathbf{T}}_0 \bar{\mathbf{u}} \text{ with } \bar{\mathbf{T}}_0 = \begin{bmatrix} \boldsymbol{\Phi}_s^d & \boldsymbol{\Psi}_c \\ \mathbf{0} & \mathbf{I}_b \end{bmatrix}, \quad \bar{\mathbf{u}} = \begin{bmatrix} \mathbf{q}_s^d \\ \mathbf{u}_b \end{bmatrix}, \tag{10}$$

in which $\bar{\mathbf{T}}_0$ and $\bar{\mathbf{u}}$ are the reduced CB transformation matrix and reduced generalized coordinate vector, respectively. The overbar $(\bar{})$ denotes the approximated quantities.

The reduced matrices of the CB method could be obtained as

$$\bar{\mathbf{M}} = \bar{\mathbf{T}}_0^T \mathbf{M}_g \bar{\mathbf{T}}_0, \quad \bar{\mathbf{K}} = \bar{\mathbf{T}}_0^T \mathbf{K}_g \bar{\mathbf{T}}_0, \tag{11}$$

and then the reduced eigenvalue problem in the CB method is given by

$$\bar{\mathbf{K}}(\bar{\boldsymbol{\varphi}})_i = \bar{\lambda}_i \bar{\mathbf{M}}(\bar{\boldsymbol{\varphi}})_i \text{ for } i = 1, 2, \ldots, \bar{N}, \tag{12}$$

where $\bar{\lambda}_i$ and $(\bar{\boldsymbol{\varphi}})_i$ are the approximated eigenvalues and eigenvectors, respectively, and $\bar{N}$ is the number of DOFs in the reduced model ($\bar{N} = N_d + N_b$). Here, N_d and N_b are the numbers of dominant substructural modes and interface boundary DOFs, respectively.

Using the eigenvectors obtained from the reduced eigenvalue problem in Eq. (12), $\bar{\mathbf{u}}$ is defined as

$$\bar{\mathbf{u}} = \bar{\boldsymbol{\Phi}} \bar{\mathbf{q}}, \tag{13}$$

in which $\bar{\boldsymbol{\Phi}}$ is the approximated eigenvector matrix that contains all the approximated eigenvectors $(\bar{\boldsymbol{\varphi}})_i$, and $\bar{\mathbf{q}}$ is the corresponding generalized coordinate vector.

In the CB method, using the reduced transformation matrix $\bar{\mathbf{T}}_0$, the approximated global eigenvector matrix $\bar{\boldsymbol{\Phi}}_g$ is defined as

$$\bar{\boldsymbol{\Phi}}_g = \bar{\mathbf{T}}_0 \bar{\boldsymbol{\Phi}}, \quad (\bar{\boldsymbol{\varphi}}_g)_i = \bar{\mathbf{T}}_0 \bar{\boldsymbol{\varphi}}_i. \tag{14}$$

3. Simplified error estimator

In this section, we briefly review the enhanced transformation matrix that is the key ingredient of the error estimator; then we summarize the original error estimator for the CB method [1], and derive a simplified error estimator.

3.1. Enhanced transformation matrix

Substituting Eq. (9) into Eq. (1) and pre-multiplying $\mathbf{T}_0^T$, the transformed equations of motion considering all the substructural modes are obtained as follows:

$$\mathbf{M}\ddot{\mathbf{u}} + \mathbf{K}\mathbf{u} = \mathbf{0}, \tag{15}$$

$$\begin{aligned} \mathbf{M} &= \mathbf{T}_0^T \mathbf{M}_g \mathbf{T}_0 = \begin{bmatrix} \mathbf{I}_s^d & \mathbf{0} & (\boldsymbol{\Phi}_s^d)^T \hat{\mathbf{M}}_c \\ \mathbf{0} & \mathbf{I}_s^r & (\boldsymbol{\Phi}_s^r)^T \hat{\mathbf{M}}_c \\ \hat{\mathbf{M}}_c^T (\boldsymbol{\Phi}_s^d) & \hat{\mathbf{M}}_c^T (\boldsymbol{\Phi}_s^r) & \hat{\mathbf{M}}_b \end{bmatrix}, \\ \mathbf{K} &= \mathbf{T}_0^T \mathbf{K}_g \mathbf{T}_0 = \begin{bmatrix} \boldsymbol{\Lambda}_s^d & \mathbf{0} & \mathbf{0} \\ \mathbf{0} & \boldsymbol{\Lambda}_s^r & \mathbf{0} \\ \mathbf{0} & \mathbf{0} & \hat{\mathbf{K}}_b \end{bmatrix}, \end{aligned} \tag{16}$$

where the component matrices are defined by

$$\mathbf{I}_s^d = (\boldsymbol{\Phi}_s^d)^T \mathbf{M}_s (\boldsymbol{\Phi}_s^d), \quad \mathbf{I}_s^r = (\boldsymbol{\Phi}_s^r)^T \mathbf{M}_s (\boldsymbol{\Phi}_s^r), \tag{17a}$$

$$\hat{\mathbf{M}}_b = \mathbf{M}_b + \mathbf{M}_c \boldsymbol{\Psi}_c + \boldsymbol{\Psi}_c^T \hat{\mathbf{M}}_c, \quad \hat{\mathbf{M}}_c = \mathbf{M}_c + \mathbf{M}_s \boldsymbol{\Psi}_c, \tag{17b}$$

$$\boldsymbol{\Lambda}_s^d = (\boldsymbol{\Phi}_s^d)^T \mathbf{K}_s (\boldsymbol{\Phi}_s^d), \quad \boldsymbol{\Lambda}_s^r = (\boldsymbol{\Phi}_s^r)^T \mathbf{K}_s (\boldsymbol{\Phi}_s^r), \quad \hat{\mathbf{K}}_b = \mathbf{K}_b + \mathbf{K}_c^T \boldsymbol{\Psi}_c. \tag{17c}$$

Note that the dominant and residual eigenvector matrices, $\boldsymbol{\Phi}_s^d$ and $\boldsymbol{\Phi}_s^r$, are orthogonal for the mass matrix $\mathbf{M}_s$ and stiffness matrix $\mathbf{K}_s$. Thus, in Eq. (16), the off-diagonal component matrices $((\boldsymbol{\Phi}_s^d)^T \mathbf{M}_s (\boldsymbol{\Phi}_s^r), (\boldsymbol{\Phi}_s^r)^T \mathbf{M}_s (\boldsymbol{\Phi}_s^d), (\boldsymbol{\Phi}_s^d)^T \mathbf{K}_s (\boldsymbol{\Phi}_s^r)$ and $(\boldsymbol{\Phi}_s^r)^T \mathbf{K}_s (\boldsymbol{\Phi}_s^d))$ become zero matrices.

Using $\ddot{(\cdot)} = d^2()/dt^2 = -\lambda()$, Eq. (15) is rewritten as

$$\begin{bmatrix} \boldsymbol{\Lambda}_s^d - \lambda \mathbf{I}_s^d & \mathbf{0} & -\lambda (\boldsymbol{\Phi}_s^d)^T \hat{\mathbf{M}}_c \\ \mathbf{0} & \boldsymbol{\Lambda}_s^r - \lambda \mathbf{I}_s^r & -\lambda (\boldsymbol{\Phi}_s^r)^T \hat{\mathbf{M}}_c \\ -\lambda \hat{\mathbf{M}}_c^T (\boldsymbol{\Phi}_s^d) & -\lambda \hat{\mathbf{M}}_c^T (\boldsymbol{\Phi}_s^r) & \hat{\mathbf{K}}_b - \lambda \hat{\mathbf{M}}_b \end{bmatrix} \begin{bmatrix} \mathbf{q}_s^d \\ \mathbf{q}_s^r \\ \mathbf{u}_b \end{bmatrix} = \mathbf{0}. \tag{18}$$

From the second row in Eq. (18), $\mathbf{q}_s^r$ can be defined

$$\mathbf{q}_s^r = \lambda (\boldsymbol{\Lambda}_s^r - \lambda \mathbf{I}_s^r)^{-1} (\boldsymbol{\Phi}_s^r)^T \hat{\mathbf{M}}_c \mathbf{u}_b. \tag{19}$$

Substituting Eq. (19) into Eq. (9) and neglecting higher order terms of λ, the global displacement vector $\mathbf{u}_g$ is approximated by

$$\mathbf{u}_g \approx \bar{\mathbf{u}}_g = \bar{\mathbf{T}}_1 \bar{\mathbf{u}} \text{ with } \bar{\mathbf{T}}_1 = \bar{\mathbf{T}}_0 + \lambda \mathbf{T}_a, \tag{20}$$

in which $\bar{\mathbf{T}}_1$ is the enhanced transformation matrix, $\bar{\mathbf{T}}_0$ is the CB transformation matrix defined in Eq. (10).

In Eq. (20), the additional transformation matrix $\mathbf{T}_a$ is given by

$$\mathbf{T}_a = \begin{bmatrix} \mathbf{0} & \mathbf{F}_{rs} \hat{\mathbf{M}}_c \\ \mathbf{0} & \mathbf{0} \end{bmatrix} \text{ with } \mathbf{F}_{rs} = (\boldsymbol{\Phi}_s^r)(\boldsymbol{\Lambda}_s^r)^{-1} (\boldsymbol{\Phi}_s^r)^T = \mathbf{K}_s^{-1} - (\boldsymbol{\Phi}_s^d)(\boldsymbol{\Lambda}_s^d)^{-1} (\boldsymbol{\Phi}_s^d)^T, \tag{21}$$

where $\mathbf{F}_{rs}$ is the static term of the residual flexibility matrix [1], and $\mathbf{K}_s^{-1}$ and $(\boldsymbol{\Phi}_s^d)(\boldsymbol{\Lambda}_s^d)^{-1} (\boldsymbol{\Phi}_s^d)^T$ are the full and dominant flexibility matrices for substructures, respectively.

It is important to note that the term $\mathbf{T}_a$ in the enhanced transformation matrix contains the effect of the residual substructural modes $\boldsymbol{\Phi}_s^r$. However, in the original transformation matrix of the CB method ($\bar{\mathbf{T}}_0$), the residual substructural modes are simply truncated without any consideration. For this reason, the enhanced transformation matrix $\bar{\mathbf{T}}_1$ can more accurately approximate the global displacement vector. The enhanced transformation matrix is essential for developing the error estimation method. However, $\bar{\mathbf{T}}_1$ could not be used to construct the reduced model without a proper treatment because it contains the unknown λ [27,28].

3.2. Original error estimator

In CMS methods, to verify the reliability of reduced models, the relative eigenvalue error could be employed

$$\xi_i = \frac{\bar{\lambda}_i - \lambda_i}{\lambda_i} = \frac{\bar{\lambda}_i}{\lambda_i} - 1, \tag{22}$$

in which ξ_i denotes the relative eigenvalue error for the ith global mode, and the exact global eigenvalue λ_i and approximated eigenvalue $\bar{\lambda}_i$ are calculated from Eqs. (3) and (12), respectively.

From the eigenvalue problem in Eq. (3), the following relation is obtained

$$\frac{1}{\lambda_i} (\boldsymbol{\varphi}_g)_i^T \mathbf{K}_g (\boldsymbol{\varphi}_g)_i = (\boldsymbol{\varphi}_g)_i^T \mathbf{M}_g (\boldsymbol{\varphi}_g)_i, \tag{23}$$

where the exact global eigensolutions, λ_i and $(\boldsymbol{\varphi}_g)_i$, satisfy the mass-orthonormality and stiffness orthogonality conditions.

The exact global eigenvector $(\boldsymbol{\varphi}_g)_i$ can be approximated using the enhanced transformation matrix $\bar{\mathbf{T}}_1$

$$(\boldsymbol{\varphi}_g)_i \approx \bar{\mathbf{T}}_1 \bar{\boldsymbol{\varphi}}_i = [\bar{\mathbf{T}}_0 + \lambda_i \mathbf{T}_a] \bar{\boldsymbol{\varphi}}_i. \tag{24}$$

Using Eq. (24) in Eq. (23), the following equation is obtained

$$\frac{1}{\lambda_i} \bar{\boldsymbol{\varphi}}_i^T [\bar{\mathbf{T}}_0 + \lambda_i \mathbf{T}_a]^T \mathbf{K}_g [\bar{\mathbf{T}}_0 + \lambda_i \mathbf{T}_a] \bar{\boldsymbol{\varphi}}_i \approx \bar{\boldsymbol{\varphi}}_i^T [\bar{\mathbf{T}}_0 + \lambda_i \mathbf{T}_a]^T \mathbf{M}_g [\bar{\mathbf{T}}_0 + \lambda_i \mathbf{T}_a] \bar{\boldsymbol{\varphi}}_i, \tag{25}$$

and its expansion results in

$$\frac{1}{\lambda_i}\bar{\boldsymbol{\varphi}}_i^T\bar{\mathbf{K}}\bar{\boldsymbol{\varphi}}_i+\bar{\boldsymbol{\varphi}}_i^T[\bar{\mathbf{T}}_0^T\mathbf{K}_g\mathbf{T}_a+\mathbf{T}_a^T\mathbf{K}_g\bar{\mathbf{T}}_0+\lambda_i\mathbf{T}_a^T\mathbf{K}_g\mathbf{T}_a]\bar{\boldsymbol{\varphi}}_i \approx \bar{\boldsymbol{\varphi}}_i^T\bar{\mathbf{M}}\bar{\boldsymbol{\varphi}}_i+\bar{\boldsymbol{\varphi}}_i^T[\lambda_i\bar{\mathbf{T}}_0^T\mathbf{M}_g\mathbf{T}_a+\lambda_i\mathbf{T}_a^T\mathbf{M}_g\bar{\mathbf{T}}_0+\lambda_i^2\mathbf{T}_a^T\mathbf{M}_g\mathbf{T}_a]\bar{\boldsymbol{\varphi}}_i. \tag{26}$$

Since $\bar{\boldsymbol{\varphi}}_i^T\bar{\mathbf{K}}\bar{\boldsymbol{\varphi}}_i=\bar{\lambda}_i$ and $\bar{\boldsymbol{\varphi}}_i^T\bar{\mathbf{M}}\bar{\boldsymbol{\varphi}}_i=1$, Eq. (26) is rewritten as

$$\frac{\bar{\lambda}_i}{\lambda_i}-1\approx\bar{\boldsymbol{\varphi}}_i^T[\lambda_i\bar{\mathbf{T}}_0^T\mathbf{M}_g\mathbf{T}_a+\lambda_i\mathbf{T}_a^T\mathbf{M}_g\bar{\mathbf{T}}_0+\lambda_i^2\mathbf{T}_a^T\mathbf{M}_g\mathbf{T}_a-\bar{\mathbf{T}}_0^T\mathbf{K}_g\mathbf{T}_a-\mathbf{T}_a^T\mathbf{K}_g\bar{\mathbf{T}}_0-\lambda_i\mathbf{T}_a^T\mathbf{K}_g\mathbf{T}_a]\bar{\boldsymbol{\varphi}}_i. \tag{27}$$

In Eq. (27), the scalar terms $\bar{\boldsymbol{\varphi}}_i^T\bar{\mathbf{T}}_0^T\mathbf{M}_g\mathbf{T}_a\bar{\boldsymbol{\varphi}}_i$ and $\bar{\boldsymbol{\varphi}}_i^T\bar{\mathbf{T}}_0^T\mathbf{K}_g\mathbf{T}_a\bar{\boldsymbol{\varphi}}_i$ are equal to $\bar{\boldsymbol{\varphi}}_i^T\mathbf{T}_a^T\mathbf{M}_g\bar{\mathbf{T}}_0\bar{\boldsymbol{\varphi}}_i$ and $\bar{\boldsymbol{\varphi}}_i^T\mathbf{T}_a^T\mathbf{K}_g\bar{\mathbf{T}}_0\bar{\boldsymbol{\varphi}}_i$, respectively. Therefore, Eq. (27) becomes

$$\frac{\bar{\lambda}_i}{\lambda_i}-1\approx 2\bar{\boldsymbol{\varphi}}_i^T\bar{\mathbf{T}}_0^T[\lambda_i\mathbf{M}_g-\mathbf{K}_g]\mathbf{T}_a\bar{\boldsymbol{\varphi}}_i+\bar{\boldsymbol{\varphi}}_i^T\mathbf{T}_a^T[\lambda_i^2\mathbf{M}_g-\lambda_i\mathbf{K}_g]\mathbf{T}_a\bar{\boldsymbol{\varphi}}_i, \tag{28}$$

in which the left side is the relative eigenvalue error ξ_i in Eq. (22).

Using $\bar{\lambda}_i$ instead of unknown λ_i in Eq. (28), the relative eigenvalue error ξ_i could be approximated as

$$\frac{\bar{\lambda}_i}{\lambda_i}-1\approx\eta_i$$

with $\eta_i=2\bar{\boldsymbol{\varphi}}_i^T\bar{\mathbf{T}}_0^T[\bar{\lambda}_i\mathbf{M}_g-\mathbf{K}_g]\mathbf{T}_a\bar{\boldsymbol{\varphi}}_i+\bar{\boldsymbol{\varphi}}_i^T\mathbf{T}_a^T[\bar{\lambda}_i^2\mathbf{M}_g-\bar{\lambda}_i\mathbf{K}_g]\mathbf{T}_a\bar{\boldsymbol{\varphi}}_i$, (29)

in which η_i is the original error estimator for the ith global mode. It can be used to evaluate the accuracy of the approximated eigenvalue $\bar{\lambda}_i$ without knowing the original eigenvalue λ_i. Its estimation accuracy and computational efficiency were tested in previous work [1]. This general conceptual idea of the error estimator could be also employed for the DOFs based model reduction techniques [29].

3.3. New error estimator

Only simple matrix and vector operations are required in the original error estimation method, see Eq. (29). However, when problems with large DOFs are handled, computational costs may become significant because there are four matrices of global DOF size, $\mathbf{M}_g$ and $\mathbf{K}_g$ ($N_g\times N_g$ matrices), and $\bar{\mathbf{T}}_0$ and $\mathbf{T}_a$ ($N_g\times\bar{N}$ matrices). To solve this problem, we approximate the original formulation in Eq. (29), and then newly derive a simplified formulation.

The error estimator η_i in Eq. (29) is rewritten as

$$\eta_i=\bar{\boldsymbol{\varphi}}_i^T[2\bar{\lambda}_i\bar{\mathbf{T}}_0^T\mathbf{M}_g\mathbf{T}_a-2\bar{\mathbf{T}}_0^T\mathbf{K}_g\mathbf{T}_a+\bar{\lambda}_i^2\mathbf{T}_a^T\mathbf{M}_g\mathbf{T}_a-\bar{\lambda}_i\mathbf{T}_a^T\mathbf{K}_g\mathbf{T}_a]\bar{\boldsymbol{\varphi}}_i. \tag{30}$$

Using $\bar{\mathbf{T}}_0$ in Eq. (10) and $\mathbf{T}_a$ in Eq. (21), $\bar{\mathbf{T}}_0^T\mathbf{M}_g\mathbf{T}_a$ and $\bar{\mathbf{T}}_0^T\mathbf{K}_g\mathbf{T}_a$ in Eq. (30) are represented in the component matrix form as follows

$$\bar{\mathbf{T}}_0^T\mathbf{M}_g\mathbf{T}_a=\begin{bmatrix}\mathbf{0}&\mathbf{A}_c\\ \mathbf{0}&\mathbf{A}_b\end{bmatrix}\ \text{with}\ \mathbf{A}_c=(\boldsymbol{\Phi}_s^d)^T\mathbf{M}_s\mathbf{F}_{rs}\hat{\mathbf{M}}_c,\quad \mathbf{A}_b=\hat{\mathbf{M}}_c^T\mathbf{F}_{rs}\hat{\mathbf{M}}_c, \tag{31a}$$

$$\bar{\mathbf{T}}_0^T\mathbf{K}_g\mathbf{T}_a=\begin{bmatrix}\mathbf{0}&\mathbf{B}_c\\ \mathbf{0}&\mathbf{B}_b\end{bmatrix}\ \text{with}\ \mathbf{B}_c=(\boldsymbol{\Phi}_s^d)^T\mathbf{K}_s\mathbf{F}_{rs}\hat{\mathbf{M}}_c,\quad \mathbf{B}_b=(\boldsymbol{\Psi}_c^T\mathbf{K}_s+\mathbf{K}_c^T)\mathbf{F}_{rs}\hat{\mathbf{M}}_c. \tag{31b}$$

Since $\boldsymbol{\Phi}_s^d$ and $\mathbf{F}_{rs}$ have orthogonality for the mass matrix $\mathbf{M}_s$ and stiffness matrix $\mathbf{K}_s$, we can identify that $(\boldsymbol{\Phi}_s^d)^T\mathbf{M}_s\mathbf{F}_{rs}=\mathbf{0}$ and $(\boldsymbol{\Phi}_s^d)^T\mathbf{K}_s\mathbf{F}_{rs}=\mathbf{0}$ in the matrices $\mathbf{A}_c$ and $\mathbf{B}_c$. In addition, using $\boldsymbol{\Psi}_c$ in Eq. (6), it is identified that $\boldsymbol{\Psi}_c^T\mathbf{K}_s+\mathbf{K}_c^T=\mathbf{0}$ in $\mathbf{B}_b$ matrix. Then, Eq. (31) is rewritten as

$$\bar{\mathbf{T}}_0^T\mathbf{M}_g\mathbf{T}_a=\begin{bmatrix}\mathbf{0}&\mathbf{0}\\ \mathbf{0}&\mathbf{A}_b\end{bmatrix}, \tag{32a}$$

$$\bar{\mathbf{T}}_0^T\mathbf{K}_g\mathbf{T}_a=\mathbf{0}. \tag{32b}$$

In addition, substituting $\mathbf{T}_a$ into $\mathbf{T}_a^T\mathbf{K}_g\mathbf{T}_a$ in Eq. (30), we have the following relation:

$$\bar{\mathbf{T}}_0^T\mathbf{M}_g\mathbf{T}_a=\mathbf{T}_a^T\mathbf{K}_g\mathbf{T}_a. \tag{33}$$

Using Eqs. (32) and (33), Eq. (30) is rewritten as

$$\eta_i=\bar{\lambda}_i\bar{\boldsymbol{\varphi}}_i^T\begin{bmatrix}\mathbf{0}&\mathbf{0}\\ \mathbf{0}&\mathbf{A}_b\end{bmatrix}\bar{\boldsymbol{\varphi}}_i+\bar{\lambda}_i^2\bar{\boldsymbol{\varphi}}_i^T\mathbf{T}_a^T\mathbf{M}_g\mathbf{T}_a\bar{\boldsymbol{\varphi}}_i. \tag{34}$$

The approximated eigenvector $\bar{\boldsymbol{\varphi}}_i$ in Eq. (34) can be partitioned as

$$\bar{\boldsymbol{\varphi}}_i=\begin{bmatrix}\bar{\boldsymbol{\varphi}}_s\\ \bar{\boldsymbol{\varphi}}_b\end{bmatrix}_i, \tag{35}$$

where $(\bar{\boldsymbol{\varphi}}_s)_i$ and $(\bar{\boldsymbol{\varphi}}_b)_i$ are the substructural and interface boundary terms of the approximated eigenvector $\bar{\boldsymbol{\varphi}}_i$, respectively.

Neglecting the second order term of $\bar{\lambda}_i$ and using Eq. (35), Eq. (34) can be approximated as

$$\eta_i\approx\mu_i=\bar{\lambda}_i(\bar{\boldsymbol{\varphi}}_b)_i^T\mathbf{A}_b(\bar{\boldsymbol{\varphi}}_b)_i, \tag{36}$$

where μ_i is a new error estimator. Note that, since $(\bar{\boldsymbol{\varphi}}_b)_i$ and $\mathbf{A}_b$ are $N_b\times 1$ vector and $N_b\times N_b$ matrix, we do not need to handle the matrices of global DOF size.

The new error estimator μ_i could be more efficiently described in a substructural component matrix form. The matrices $\hat{\mathbf{M}}_c$ and $\mathbf{F}_{rs}$, parts of $\mathbf{A}_b$, are represented as

$$\hat{\mathbf{M}}_c=\begin{bmatrix}\hat{\mathbf{M}}_c^{(1)}\\ \hat{\mathbf{M}}_c^{(2)}\\ \vdots\\ \hat{\mathbf{M}}_c^{(k)}\end{bmatrix},\quad \mathbf{F}_{rs}=\begin{bmatrix}\mathbf{F}_{rs}^{(1)}&&&\mathbf{0}\\ &\mathbf{F}_{rs}^{(2)}&&\\ &&\ddots&\\ \mathbf{0}&&&\mathbf{F}_{rs}^{(k)}\end{bmatrix}$$

$$\text{with}\ \mathbf{F}_{rs}^{(k)}=(\mathbf{K}^{(k)})^{-1}-(\boldsymbol{\Phi}_d^{(k)})(\boldsymbol{\Lambda}_d^{(k)})^{-1}(\boldsymbol{\Phi}_d^{(k)})^T\ \text{for}\ k=1,2,\ldots,n, \tag{37}$$

where $\mathbf{F}_{rs}^{(k)}$ is the static term of the residual flexibility matrix for the kth substructure, and it is easily calculated by reusing $(\mathbf{K}^{(k)})^{-1}$, $\boldsymbol{\Phi}_d^{(k)}$ and $\boldsymbol{\Lambda}_d^{(k)}$ in Eqs. (6) and (7).

Then, $\mathbf{A}_b$ can be represented by the addition of the substructural matrix terms

$$\mathbf{A}_b=\sum_{k=1}^{n}\mathbf{A}_b^{(k)}\ \text{with}\ \mathbf{A}_b^{(k)}=\hat{\mathbf{M}}_c^{(k)^T}\mathbf{F}_{rs}^{(k)}\hat{\mathbf{M}}_c^{(k)}. \tag{38}$$

Due to symmetry, $\mathbf{F}_{rs}^{(k)}$ in Eq. (38) can be decomposed into three parts

$$\mathbf{F}_{rs}^{(k)}=\mathbf{F}_d^{(k)}+\mathbf{F}_u^{(k)}+\mathbf{F}_u^{(k)^T}\ \text{for}\ k=1,2,\ldots,n, \tag{39}$$

in which $\mathbf{F}_d^{(k)}$ and $\mathbf{F}_u^{(k)}$ are the diagonal and upper triangular parts of $\mathbf{F}_{rs}^{(k)}$, respectively.

Finally, using Eqs. (36), (38) and (39), the new error estimator μ_i for the ith relative eigenvalue error is redefined by

$$\mu_i=\sum_{k=1}^{n}\mu_i^{(k)},\quad \mu_i^{(k)}=e_1^{(k)}+2e_2^{(k)},$$

$$\text{with}\ e_1^{(k)}=\bar{\lambda}_i(\bar{\boldsymbol{\varphi}}_b)_i^T\hat{\mathbf{M}}_c^{(k)^T}\mathbf{F}_d^{(k)}\hat{\mathbf{M}}_c^{(k)}(\bar{\boldsymbol{\varphi}}_b)_i,\quad e_2^{(k)}=\bar{\lambda}_i(\bar{\boldsymbol{\varphi}}_b)_i^T\hat{\mathbf{M}}_c^{(k)^T}\mathbf{F}_u^{(k)}\hat{\mathbf{M}}_c^{(k)}(\bar{\boldsymbol{\varphi}}_b)_i, \tag{40}$$

where $\mu_i^{(k)}$ is the estimated substructural error corresponding to the kth substructure for ith relative eigenvalue error, and the new error estimator μ_i is simply obtained by a summation of the substructural errors estimated.

In Eq. (40), there is no need to calculate the matrix $\mathbf{T}_a$ that is a prerequisite of the original error estimation method, and it only requires substructural component matrices such as $\hat{\mathbf{M}}_c^{(k)}$ and $\mathbf{F}_{rs}^{(k)}$.

Therefore, it is easy to identify that Eq. (40) is much more computationally efficient than the original error estimation method in Eq. (29). Details of the computational cost are presented in Section 4.

In addition, it is important to note that the estimated substructural error $\mu_i^{(k)}$ in Eq. (40) provides the contribution of the kth substructure to the ith relative eigenvalue error. Using this feature, we propose an error control strategy to improve effectively the accuracy of the global modes having relatively large errors. This strategy will be presented in Section 5.

4. Numerical examples

In this section, to investigate the performance of the new error estimator, we consider three practical engineering problems involving a stiffened plate, a cargo hold structure, and a semi-submersible rig.

All FE (Finite Element) models are constructed using the 4-node MITC shell element [30–32], and the free boundary condition is imposed. Here, we use the material property of a mild steel, so that Young's modulus E, Poisson's ratio υ and density ρ are 206 GPa, 0.3, and 7850 kg/m^3, respectively. The frequency cut-off method is employed to select the dominant substructural modes [3]. All the code implementations are done using MATLAB in a personal computer (Intel core (TM) i7-3770, 3.40 GHz CPU, 32 GB RAM).

4.1. Stiffened plate problem

Here, we consider a stiffened plate, an important component of ships (see Fig. 2). Length L, breadth B, and stiffener spacing S are 26.0 m, 6.0 m, and 2.0 m, respectively. The stiffener is composed of a vertical web of height 0.05 m and a flange of breadth 0.02 m, and the thickness t is 0.019 m. The number of DOFs is 52662 and the global structure is partitioned into 18 substructures. For two numerical cases, we use 60 and 200 dominant substructural modes ($N_d = 60$ and $N_d = 200$).

The exact and estimated relative eigenvalue errors calculated by the previous (original) and present formulations are plotted in Fig. 3 for the two numerical cases. The estimated relative eigenvalue errors are also compared with those calculated by the error estimation method developed by Elssel and Voss [21],

$$\hat{\mu}_i = \frac{\bar{\lambda}_i}{|\lambda_r - \bar{\lambda}_i|}, \tag{41}$$

where λ_r is the smallest residual eigenvalue of substructures.

Table 1 lists the exact and estimated relative eigenvalue errors corresponding to Fig. 3(a). This clearly shows that the accuracy of the present formulation is very similar to its original formulation. Table 2 shows the details of computational cost corresponding to Fig. 3(a). Compared to the computation time required for the CB method, the original formulation requires 35.85% of additional computation time. On the other hand, the present formulation only requires 2.27% of additional computation time.

Although the error estimation method developed by Elssel and Voss gives the tendency of the relative eigenvalue error as an upper bound, its estimation capability is not adequate for practical use in engineering problems. However, it requires almost no computational cost, because it is an *a priori* method and a scalar operation technique.

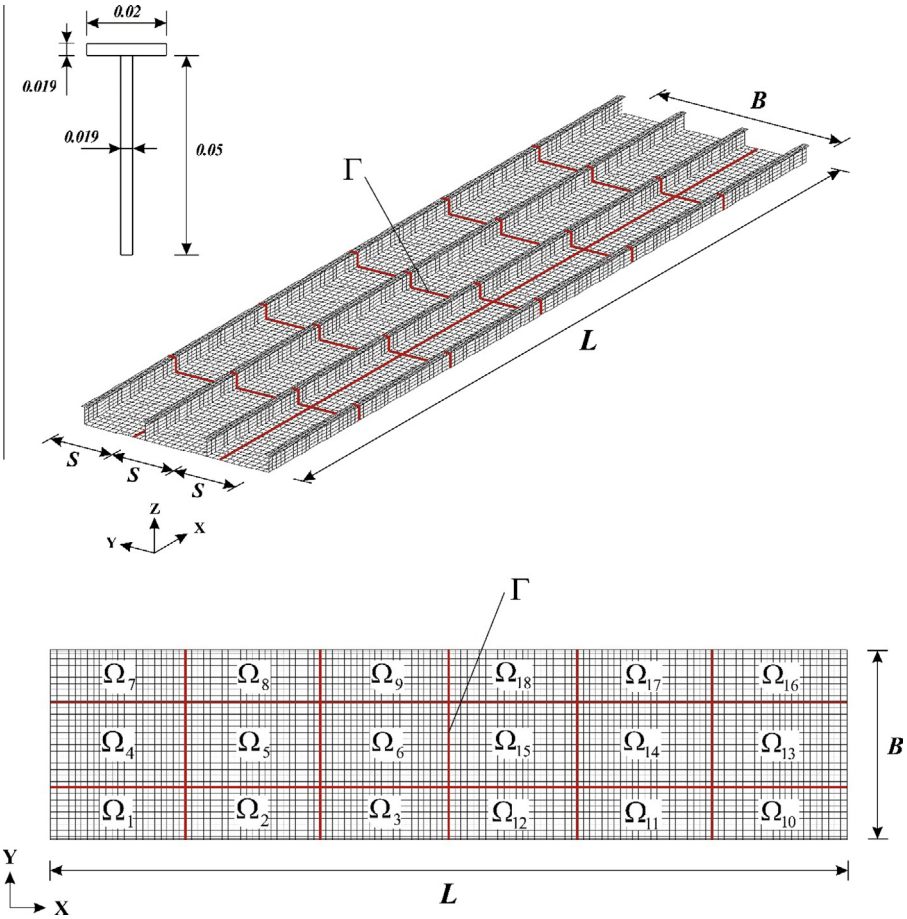

Fig. 2. Stiffened plate problem.

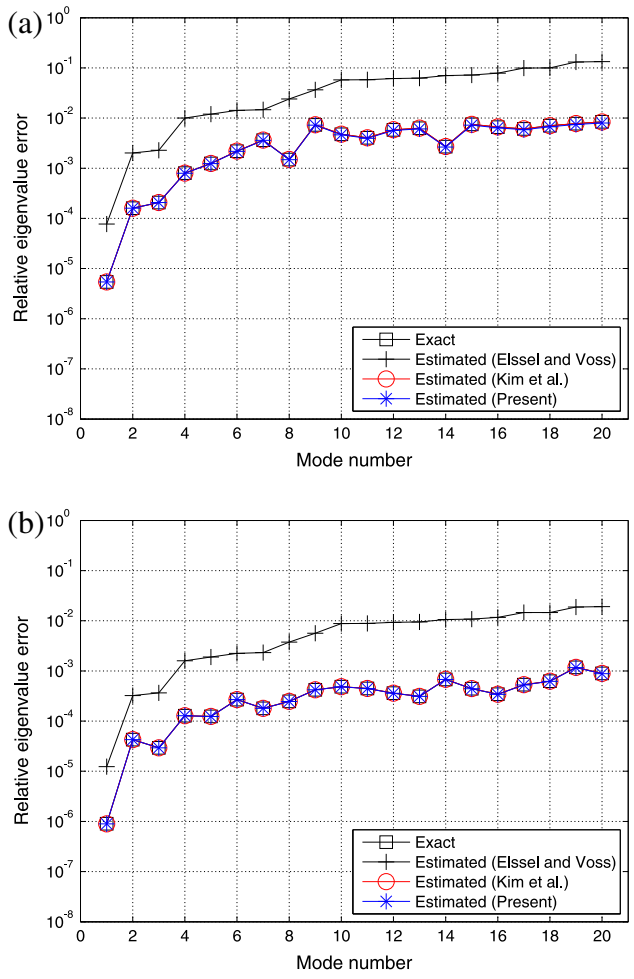

Fig. 3. Exact and estimated relative eigenvalue errors for the stiffened plate problem: (a) $N_d = 60$ and (b) $N_d = 200$.

Table 1
Exact and estimated relative eigenvalue errors in the stiffened plate problem in Fig. 3(a).

Mode number	Exact	Estimated	
		Previous	Present
1	0.00001	0.00001	0.00001
2	0.00016	0.00016	0.00016
3	0.00021	0.00021	0.00021
4	0.00080	0.00080	0.00079
5	0.00125	0.00125	0.00124
6	0.00218	0.00219	0.00217
7	0.00362	0.00363	0.00360
8	0.00149	0.00149	0.00148
9	0.00730	0.00737	0.00721
10	0.00474	0.00477	0.00463
11	0.00404	0.00405	0.00394
12	0.00582	0.00585	0.00567
13	0.00627	0.00629	0.00607
14	0.00269	0.00270	0.00264
15	0.00748	0.00748	0.00721
16	0.00658	0.00668	0.00640
17	0.00609	0.00611	0.00586
18	0.00703	0.00705	0.00672
19	0.00774	0.00778	0.00744
20	0.00843	0.00839	0.00795

Considering symmetric partitioning, the computational cost for the present error estimator could be reduced more. As shown in Fig. 2, the substructures 1, 2, 3, 4, 5, and 6 are symmetric with

Table 2
Specific computational cost for the stiffened structure problem in Fig. 3(a).

Items		Computation times	
		[sec]	Ratio [%]
CB method		165.24	100.00
Previous error estimator in Eq. (29)	Calculation of the residual flexibility matrix $\mathbf{F}_{rs}$	1.89	1.14
	Calculation of $\mathbf{T}_a$ matrix	41.12	24.89
	Calculation error estimator η_i	16.23	9.82
	Total	59.24	35.85
Present error estimator in Eq. (40)	Calculation of the residual flexibility matrix $\mathbf{F}_{rs}$	1.89	1.14
	Calculation error estimator μ_i	1.87	1.13
	Total	3.76	2.27
Present error estimator considering symmetric partitioning	Calculation of the residual flexibility matrix $\mathbf{F}_{rs}$	0.79	0.48
	Calculation error estimator μ_i	0.40	0.24
	Total	1.19	0.72
Elssel and Voss's error estimator in Eq. (41)		0.000011	0.0000066

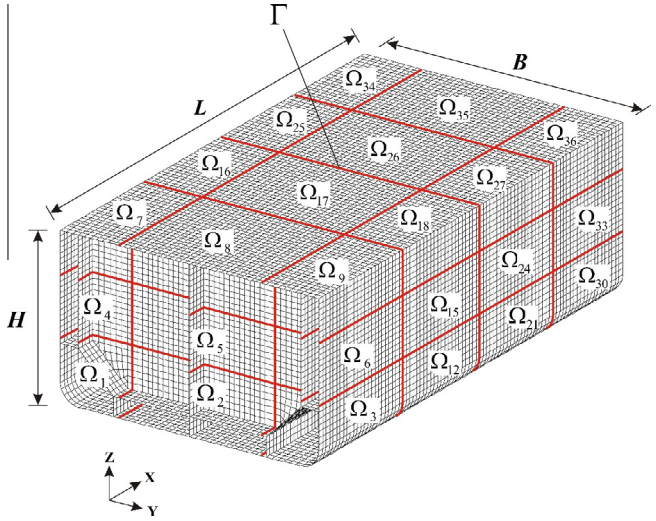

Fig. 4. Cargo hold structure problem.

the other substructures. Thus, it is necessary to calculate the residual flexibility $\mathbf{F}_{rs}$ and substructural error $\mu_i^{(k)}$ only for the substructures 1, 2, 3, 4, 5, and 6. The computational cost for the present error estimator, considering symmetric partitioning, is also presented in Table 2.

4.2. Cargo hold structure problem

Here, a cargo hold structure of an oil carrier is considered (shown in Fig. 4). The height H, breadth B, length L, and thickness t are 30.0 m, 50.0 m, 87.0 m, and 0.025 m, respectively. We use 26761 shell elements and 26228 nodes for finite element modeling. The number of total DOFs is 157368, and the global structure is partitioned into 36 substructures. Two different retained substructural mode cases, $N_d = 80$ and $N_d = 290$, are considered here.

Fig. 5 shows the exact and estimated relative eigenvalue errors calculated by the previous and present formulations in the two

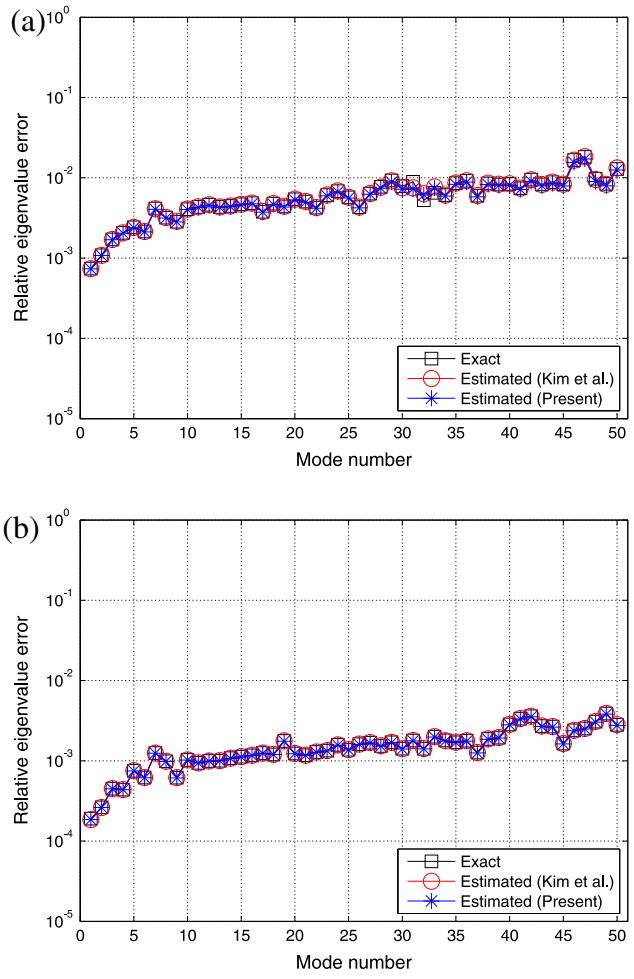

Fig. 5. Exact and estimated relative eigenvalue errors for the cargo hold structure problem: (a) $N_d = 80$ and (b) $N_d = 290$.

Table 3
Computational cost for the cargo hold structure problem in Fig. 5(a).

Items	Computation times	
	[sec]	Ratio [%]
CB method	686.47	100.00
Previous error estimator in Eq. (29)	374.74	54.58
Present error estimator in Eq. (40)	28.98	4.22

numerical cases. The required computational costs corresponding to Fig. 5(a) are presented in Table 3. Note that the computational cost of the original error estimator in Eq. (29) is not small when the number of DOFs is over 150000. The numerical results demonstrate the solution accuracy and computational efficiency of the present error estimation method.

4.3. Semi-submersible rig problem

We consider a semi-submersible rig problem. Breadth B and column width C are 80.0 m and 20.0 m, respectively. Heights H_1 and H_2 are 50.0 m and 15.0 m, respectively, and length L and thickness t are 110.0 m and 0.018 m, respectively. The structure is modeled using 16800 shell elements and 17009 nodes. The number of total DOFs is 105054. The global structure is partitioned into 28 substructures, see Fig. 6. Here, two different retained substructural mode cases, $N_d = 54$ and $N_d = 160$, are considered. The estimating

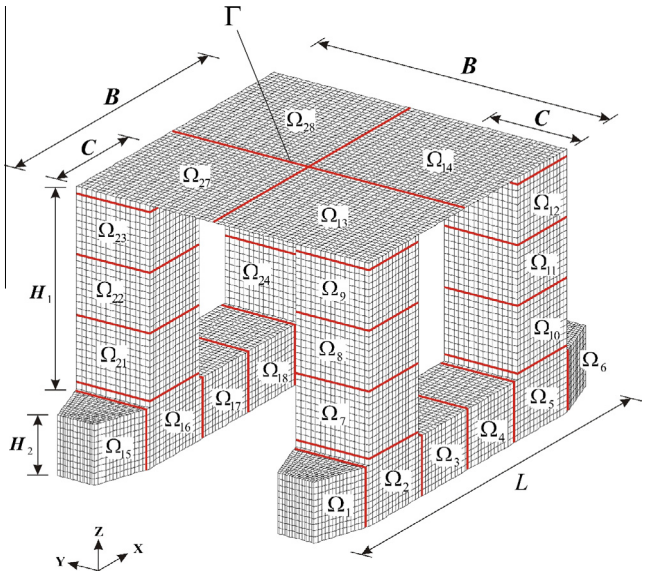

Fig. 6. Semi-submersible rig problem.

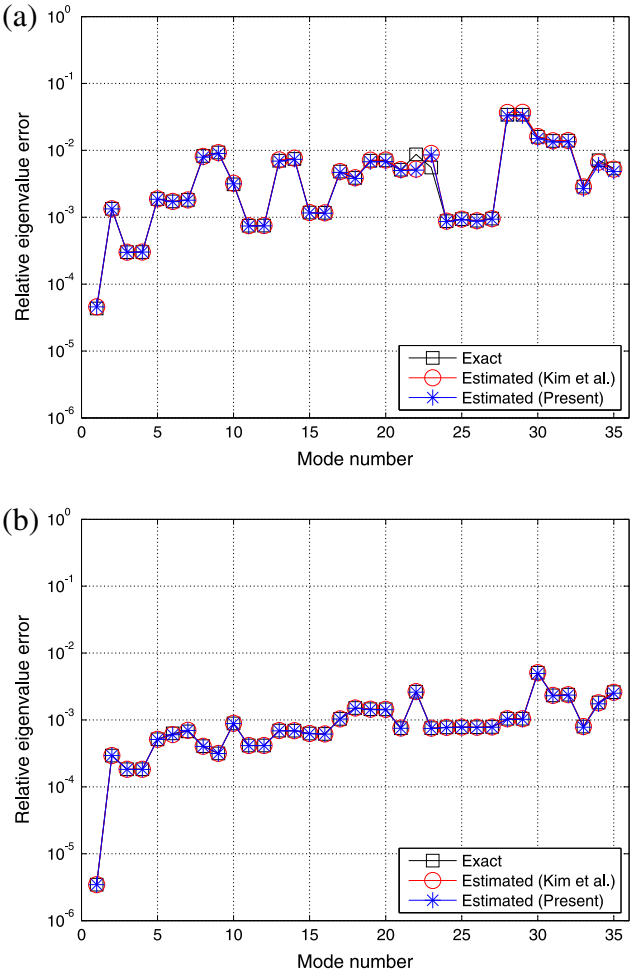

Fig. 7. Exact and estimated relative eigenvalue errors for the semi-submersible rig problem: (a) $N_d = 54$ and (b) $N_d = 160$.

accuracy and computational efficiency of the present error estimator are verified in Fig. 7 and Table 4. The computational cost is reduced a lot using the new error estimator.

Table 4
Computational cost for the semi-submersible rig problem in Fig. 7(a).

Items	Computation times	
	[sec]	Ratio [%]
CB method	575.77	100.00
Previous error estimator in Eq. (29)	176.69	30.68
Present error estimator in Eq. (40)	11.95	2.07

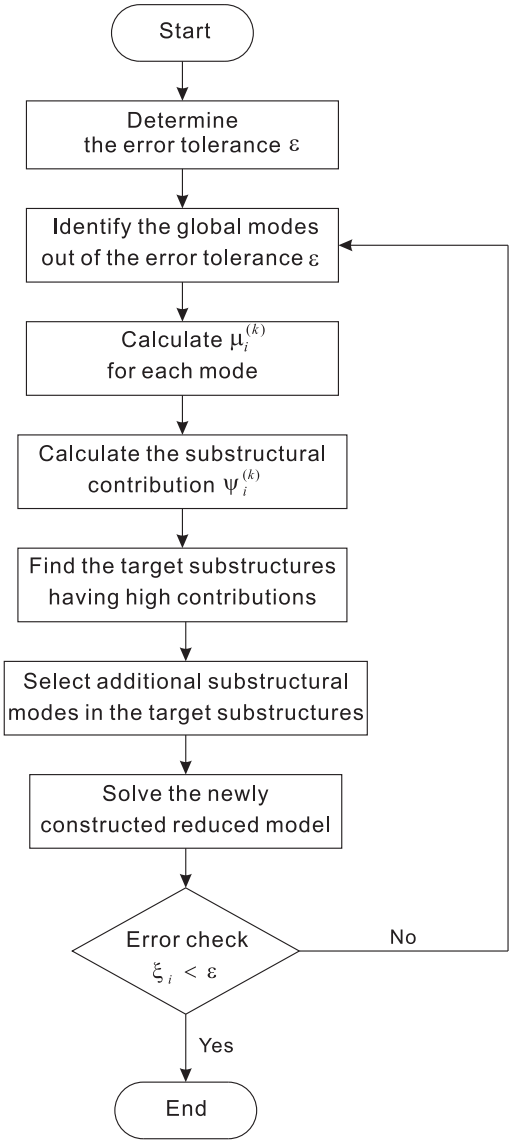

Fig. 8. Flow chart for the error control strategy.

5. Error control strategy

In this section, using the estimated substructural errors $\mu_i^{(k)}$ in Eq. (40), we suggest an error control strategy to improve the accuracy of the global modes having relatively large errors. In this strategy, it is important to calculate the substructural contributions to the selected global modes, and the substructural contribution is defined as

$$\psi_i^{(k)} = \frac{\mu_i^{(k)}}{\mu_i} \times 100\ [\%], \tag{42}$$

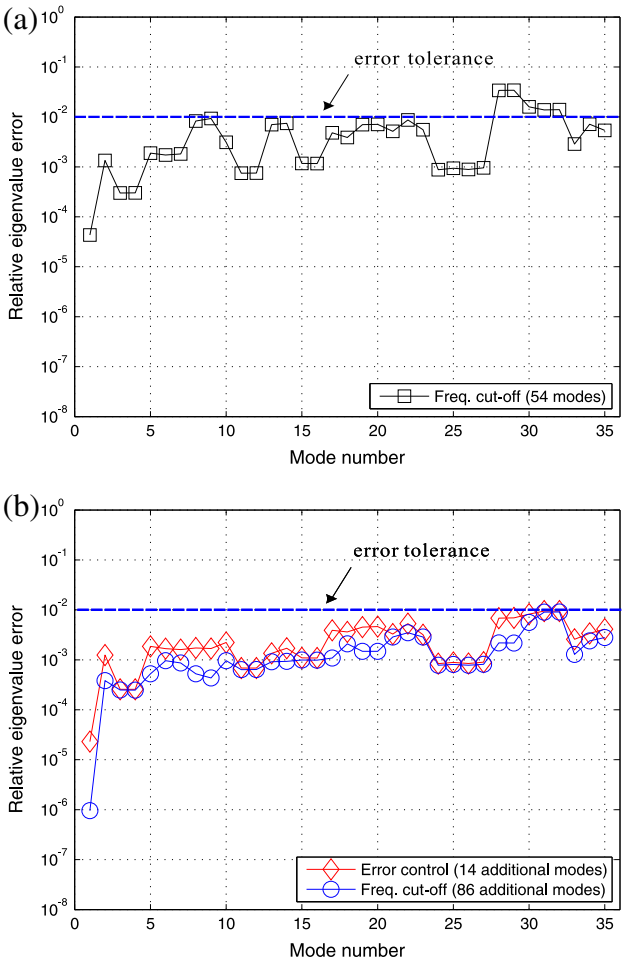

Fig. 9. Relative eigenvalue errors for the semi-submersible rig problem in Fig. 7(a): (a) before applying the error control strategy and (b) after applying the error control strategy.

where $\psi_i^{(k)}$ is the substructural contribution of the kth substructure to the ith global mode.

The error control strategy is simple. For the global modes of interest, the substructural contributions $\psi_i^{(k)}$ are calculated using Eq. (42). The target substructures that contain high contributions are identified, and additional substructural modes are retained only for the target substructures to construct a more precisely reduced model. The detailed procedure of the error control strategy is described in Fig. 8. Using this strategy, we can improve the accuracy of the selected global modes, resulting in an effective reduced model of small DOFs with desired accuracy.

The error control strategy is tested with the semi-submersible rig problem considering the case of $N_d = 54$, see Figs. 6 and 7(a). We assign the error tolerance 10^{-2}, and it is observed that the 28th–32th global modes are out of the error tolerance, see Fig. 9 (a). Fig. 10 and Table 5 show the substructural contributions $\psi_i^{(k)}$ to the 28th–32th global modes, and it is identified that the substructures 2, 4, 5, 13, 14, 16, 18, 19, 27, and 28 have relatively high contributions to the 28th–32th global modes. Thus, we designate those substructures as target substructures. Note that, in Fig. 10, the substructural contributions are plotted only for substructures 1–14 due to the geometrically symmetric condition.

To improve the accuracy of the global modes out of the error tolerance, for the selected target substructures, additional substructural modes are retained in the reduced model (2 additional

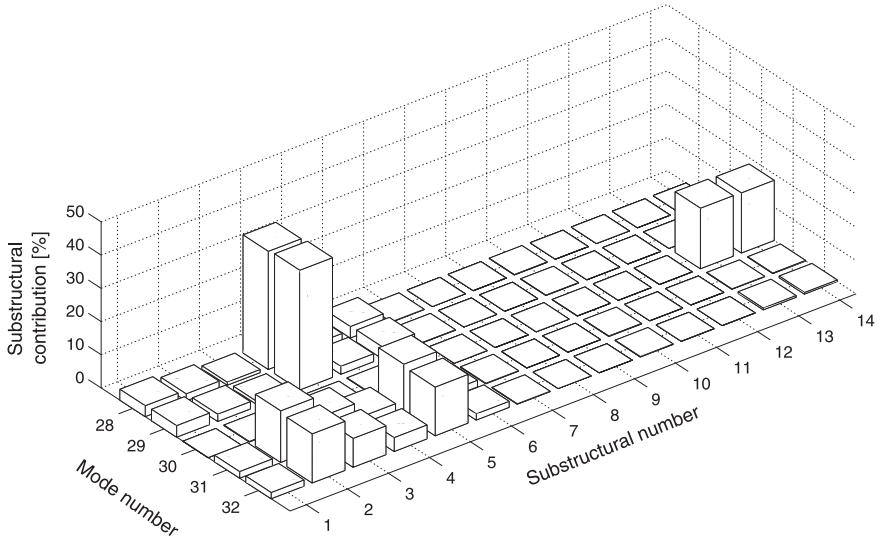

Fig. 10. Substructural contributions to the 28th–32th global mode errors for the semi-submersible rig problem in Fig. 7(a).

Table 5
Substructural contributions $\psi_i^{(k)}$ to the 28th–32th global modes for the semi-submersible rig problem in Fig. 7(a). Underlines denote relatively high substructural contributions to the 28th–32th global modes and the corresponding substructural numbers.

Substructural numbers	Substructural contributions $\psi_i^{(k)}$ (%)				
	$\psi_{28}^{(k)}$	$\psi_{29}^{(k)}$	$\psi_{30}^{(k)}$	$\psi_{31}^{(k)}$	$\psi_{32}^{(k)}$
1, 15	3.41	3.57	0.04	2.05	1.93
2, 16	2.22	2.24	0.16	16.12	15.34
3, 17	0.92	0.93	0.10	9.45	9.00
4, 18	36.84	37.35	0.09	4.61	4.32
5, 19	2.40	2.42	0.16	15.96	15.18
6, 20	3.57	3.73	0.04	2.03	1.91
7, 21	0.10	0.08	0.02	0.16	0.15
8, 22	0.00	0.00	0.00	0.01	0.01
9, 23	0.00	0.00	0.01	0.01	0.01
10, 24	0.12	0.10	0.02	0.15	0.15
11, 25	0.00	0.00	0.00	0.01	0.01
12, 26	0.00	0.00	0.01	0.01	0.01
13, 27	0.00	0.00	19.42	0.14	0.50
14, 28	0.00	0.00	19.27	0.14	0.49
Total	100.00	100.00	100.00	100.00	100.00

modes for the target substructures 2, 5, 16 and 19, and 1 additional mode for the other target substructures). Fig. 9(b) shows the result after applying the proposed error control strategy, and it is identify that the relative eigenvalue errors out of the error tolerance are effectively controlled by the proposed strategy. In Fig. 9(b), it can be seen that to satisfy the error tolerance, the pure frequency cut-off method requires 86 additional substructural modes without any strategy, while the proposed strategy requires only 14 additional substructural modes. Thus, it can be concluded that the proposed error control strategy is very effective for constructing an improved reduced model that has better accuracy with fewer substructural modes.

Note that, the relative eigenvalue errors corresponding to the 8th, 9th, 13th, and 14th global modes become also more accurate than before because the selected target substructures also have high contributions for those global modes.

It is important to note that, in this study, we only focused on the model reduction error. That is, the discretization error in original FE models was not considered. The discretization error and its estimation methods have been well studied [33–35].

6. Conclusions

In this study, we proposed a simplified error estimator for the CB method. The simplified formulation was derived by neglecting insignificant terms in the original formulation. The error estimator can be represented in the substructural component matrix level to improve computational efficiency. An important feature of the new error estimator lies in the fact that the estimated relative eigenvalue error is simple to calculate using summation of the substructural errors estimated. The substructural errors represent the contributions of individual substructures to the relative eigenvalue errors. Using this feature, we proposed an error control strategy to improve the accuracy of reduced models efficiently. Through various numerical examples, we demonstrated the accuracy and computational efficiency of the simplified error estimator, and a new error control strategy for it.

In future work, it would be valuable to develop an error estimator applicable to the CB method using the interface reduction technique and the iterative mode selection algorithms to construct accurate reduced-order models.

Acknowledgements

This work was supported by the Climate Change Research Hub of KAIST (No. N01150026), and the Human Resources Program in Energy Technology of the Korea Institute of Energy Technology Evaluation and Planning (KETEP), granted financial resource from the Ministry of Trade, Industry & Energy, Republic of Korea (No. 20134030200300).

References

[1] Kim JG, Lee KH, Lee PS. Estimating relative eigenvalue errors in the Craig–Bampton method. Comput Struct 2014;139:54–64.
[2] Hurty W. Dynamic analysis of structural systems using component modes. AIAA J 1965;3(4):678–85.
[3] Craig RR, Bampton MCC. Coupling of substructures for dynamic analysis. AIAA J 1968;6(7):1313–9.
[4] Craig RR, Hale AL. Block–Krylov component synthesis method for structural model reduction. AIAA J 1988;11(6):562–70.
[5] Craig RR. Substructure method in vibration. J Vib Acoust 1995;117(B):207–13.
[6] MacNeal RH. Hybrid method of component mode synthesis. Comput Struct 1971;1(4):581–601.
[7] Benfield WA, Hruda RF. Vibration analysis of structures by component mode substitution. AIAA J 1971;9:1255–61.

[8] Kuhar EJ, Stahle CV. Dynamic transformation method for modal synthesis. AIAA J 1974;12(5):672–8.
[9] Rubin S. Improved component-mode representation for structural dynamic analysis. AIAA J 1975;13(8):995–1006.
[10] Bourquin F. Component mode synthesis and eigenvalues of second order operators: discretization and algorithm. Math Model Numer Anal 1992;26 (3):385–423.
[11] Bourquin F, d'Hennezel F. Numerical study of an intrinsic component mode synthesis method. Comput Methods Appl Mech Eng 1992;97(1):49–76.
[12] Park KC, Park YH. Partitioned component mode synthesis via a flexibility approach. AIAA J 2004;42(6):1236–45.
[13] Rixen DJ. A dual Craig–Bampton method for dynamic substructuring. J Comput Appl Math 2004;168(1-2):383–91.
[14] Park KC, Kim JG, Lee PS. A mode selection criterion based on flexibility approach in component mode synthesis. In: Proceeding 53rd AIAA/ASME/ASCE/AHS/ASC structures, structural dynamics, and materials conference USA. Hawaii; 2012.
[15] Kim JG, Lee PS, Park KC. A mode selection algorithm for the flexibility based component mode synthesis. In: Proceedings of 5th international conference on computational methods in structural dynamics and earthquake engineering (COMPDYN 2015); 2015.
[16] John TS, Walter ST. Selection of component modes for flexible multibody simulation. AIAA J 1991;14(2):278–86.
[17] Papadimiriou C, Papadioti DC. Component mode synthesis technique for finite element model updating. Comput Struct 2013;126:15–28.
[18] Hou G, Maroju V. Component mode synthesis-based design optimization method for local structural modification. Struct Optim 1995;10:128–36.
[19] Lall S, Marsden JE, Glavaski S. A subspace approach to balanced truncation for model reduction of nonlinear control system. Int J Robust Nonlinear Control 2002;12(6):519–35.
[20] Bourquin F. Analysis and comparison of several component mode synthesis methods on one dimensional domains. Numer Math 1990;58(1):11–33.
[21] Elssel K, Voss H. An a priori bound for automated multi-level substructuring. SIAM J 2007;28(2):386–97.
[22] Jakobosson H, Larson MG. A posteriori error analysis of component mode synthesis for the elliptic eigenvalue problem. Comput Methods Appl Mech Eng 2011;200:2840–7.
[23] Kim JG, Lee PS. A posteriori error estimation method for the flexibility-based component mode synthesis. AIAA J 2015;53(10):2828–37.
[24] Bennighof JK, Kaplan MF. Frequency sweep analysis using multi-level substructuring, global modes and iteration. In: Proceedings of the 39th annual AIAA structural dynamics and materials conference. Long Beach (CA); 1998.
[25] Kaplan MF. Implementation of automated multi-level substructuring for frequency response analysis of structures [Ph.D. thesis]. Austin (TX): Department of Aerospace Engineering & Engineering Mechanics, University of Texas at Austin; 2001.
[26] Bennighof JK, Lehoucq RB. An automated multi-level substructuring method for eigenspace computation in linear elastodynamics. SIAM J Sci Comput 2004;25(6):2084–106.
[27] Kim JG, Lee PS. An enhanced Craig–Bampton method. Intl J Numer Methods Eng 2015;103:79–93.
[28] Kim JG, Boo SH, Lee PS. An enhanced AMLS method and its performance. Comput Methods Appl Mech Eng 2015;287:90–111.
[29] Kim JG, Lee PS. An accurate error estimator for Guyan reduction. Comput Methods Appl Mech Eng 2014;279:1–19.
[30] Dvorkin EN, Bathe KJ. A continuum mechanics based four-node shell element for general nonlinear analysis. Eng Comput 1984;1(1):77–88.
[31] Lee PS, Bathe KJ. Development of MITC isotropic triangular shell finite elements. Comput Struct 2004;82(11-12):945–62.
[32] Lee YG, Lee PS, Bathe KJ. The MITC3+ shell finite element and its performance. Comput Struct 2014;138:12–23.
[33] Babuvška I, Rheinboldt WC. Error estimates for adaptive finite element computations. SIAM J 1978;15(4):736–54.
[34] Rabczuk T, Belytschko T. Adaptivity for structured meshfree particle methods in 2D and 3D. Intl J Numer Methods Eng 2005;63(11):1559–82.
[35] Nguyen-Xuan H, Liu GR, Bordas S, Natarajan S, Rabczuk T. An adaptive singular ES-FEM for mechanics problems with singular field of arbitrary order. Comput Methods Appl Mech Eng 2013;253:252–73.